Journal of Computer-Aided Molecular Design, 10 (1996) 361–371
ESCOM

J-CAMD 350

CORCEMA evaluation of the potential role of intermolecular transferred NOESY in the characterization of ligand–receptor complexes

Ernest V. Curto, Hunter N.B. Moseley and N. Rama Krishna*

Department of Biochemistry and Molecular Genetics, and Comprehensive Cancer Center, The University of Alabama at Birmingham, 933 South 19th Street, Birmingham, AL 35294-2041, U.S.A.

Received 3 March 1996
Accepted 3 April 1996

Keywords: Conformational exchange; Complete relaxation matrix; CORCEMA; Hinge-bending; Transferred NOESY; Structure-based drug design by NMR; Ligand–receptor complexes

Summary

We report a theoretical characterization of the intermolecular transferred NOESY (inter-TrNOESY) between ligands and receptor macromolecules that bind reversibly, using a COmplete Relaxation and Conformational Exchange MAtrix (CORCEMA) theory developed in our laboratory. We examine the dependence of inter-TrNOESY on the dissociation constant, off-rate, ligand-to-receptor ratio, and distance variations between protons of interacting species within the complex. These factors are analyzed from simulations on two model systems: (i) neuraminidase complexed to a transition-state analogue; and (ii) thermolysin complexed to a leucine-based inhibitor. The latter case utilizes a three-state model of interaction to simulate the effect of hinge-bending motions on the inter-TrNOESY. Our calculations suggest a potential role for inter-TrNOESY (when observable) and CORCEMA analysis in properly docking the ligand within the active site, and in refining the conformation of the ligand–receptor (active-site) complex. These findings have implications on the structure-based design of ligands (e.g., inhibitors) reversibly binding to receptors (e.g., enzymes).

Introduction

The Transferred Nuclear Overhauser Effect (TrNOE) is ideally suited for determining the bound conformations of ligands forming weak complexes with large proteins [1–3]. The implicit prospect of deducing the bound conformation of a ligand *without the need for a knowledge of the binding site within the protein* was the source of much initial enthusiasm. Since then, detailed theoretical formulations have identified a number of factors that influence the intramolecular TrNOESY (intra-TrNOESY) [4–14]. In the absence of receptor–ligand cross-relaxation, the analysis of TrNOESY to obtain bound ligand conformation becomes relatively simpler. Where this situation is not realized, recent studies have shown that it is highly desirable, whenever possible, to include active-site residues in a quantitative analysis of intra-TrNOESY to account for protein-mediated spin diffusion [6,9–14] and motions in the protein–ligand complex [12–14]. Our laboratory has developed a computer program to address these issues and analyze the effects of conformational exchange on NOESY spectra using a COmplete Relaxation and Conformational Exchange MAtrix (CORCEMA) formalism [11–14].

In this report, we investigate factors governing the intermolecular TrNOESY (inter-TrNOESY). We show that, under a wide range of binding conditions, the inter-TrNOESY technique together with CORCEMA analysis is potentially useful in properly docking the ligand within the active site and, together with additional information (vide infra), in optimizing the structure of the ligand–receptor (active-site) complex. We illustrate the potential of CORCEMA analysis using two realistic models of hypothetical systems consisting of the active sites and inhibitors of neuraminidase and thermolysin. This work has been motivated because of reports of intermolecular transferred NOE contacts observed experimentally (e.g., Refs. 15–23), as well as the realization by us [11,14] and

*To whom correspondence should be addressed. A copy of the CORCEMA program may be obtained from this author.

others [10,20,21,24] that these contacts may potentially be exploited in structure refinement. Simulations of the type presented here can help clarify the complex behavior of inter-TrNOESY intensities for a wide range of conditions, and assist the experimentalist in the selection of optimal experimental conditions.

Theory

A general theory for the CORCEMA analysis of NOESY spectra of interacting systems (ligand–receptor systems) existing in multistate equilibrium is described elsewhere [14]. This theory applies to both intraligand and intrareceptor NOESY as well as inter-ligand–receptor NOESY contacts under a wide range of binding conditions. It is an extension, *to interacting systems*, of the theory of transferred NOESY for finite-exchange off-rates developed previously by us [4]. It incorporates the formalism for multistate conformational exchange [25]. A brief summary of the methodology follows. We treat the ligand

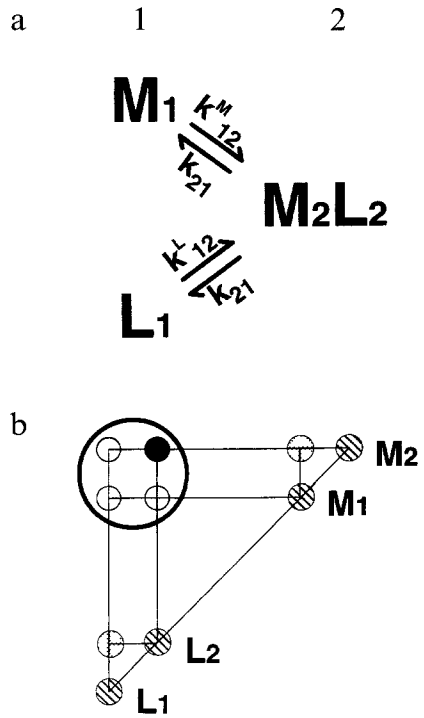

Fig. 1. (a) A two-state model of an interaction between a receptor macromolecule (M) and a reversibly bound ligand (L). (1) and (2) designate the free and bound states respectively. The parameters $k_{12}^{M} = k_{on}$ $[L_1]$ and $k_{12}^{L} = k_{on}$ $[M_1]$ are the rates at which the macromolecule and ligand enter the complex, respectively, and k_{21} is the dissociation rate of the complex (k_{off}). (b) Schematic for the NOESY spectrum of a ligand–receptor system described by a two-state model. Each small circle represents a group of peaks from protons. These are intra-NOESY (striped circles), exchange and exchange-mediated cross-peaks between the free and bound forms of a given molecule (spotted circles), exchange-mediated intermolecular Tr-NOESY (open circles) and direct intermolecular NOESY (filled circle) between ligand and receptor. The four inter-TrNOESY classes are grouped together by a large circle.

binding process as no different from a conformational exchange process, since: (i) the correlation time of the ligand changes from free to bound states; and (ii) even the conformation can change. We construct a *generalized* relaxation rate matrix **R** which describes the relaxation behavior of the entire system: the system may consist of a ligand (L) and a receptor macromolecule (M) existing in a two-state equilibrium ($L_1 + M_1 \rightleftarrows L_2M_2$) or a multistate equilibrium. For the two-state case (Fig. 1), **R** is defined as [14]:

$$\mathbf{R} = \begin{bmatrix} \mathbf{R}_1 & 0 \\ 0 & \mathbf{R}_2 \end{bmatrix} \tag{1}$$

where

$$\mathbf{R}_1 = \begin{bmatrix} \mathbf{R}_1^{L} & 0 \\ 0 & \mathbf{R}_1^{M} \end{bmatrix} \quad \text{and} \quad \mathbf{R}_2 = \begin{bmatrix} \mathbf{R}_2^{L} & \mathbf{R}_2^{LM} \\ \mathbf{R}_2^{ML} & \mathbf{R}_2^{M} \end{bmatrix} \tag{2}$$

$\mathbf{R}_1$ and $\mathbf{R}_2$ are the *generalized* relaxation rate matrices for the free and bound states, respectively, and $\mathbf{R}_1^{L}$ and $\mathbf{R}_1^{M}$ are the relaxation rate matrices for the free ligand and free macromolecule, respectively. In the bound state, $\mathbf{R}_2^{L}$ and $\mathbf{R}_2^{M}$ are the corresponding rate matrices, with $\mathbf{R}_2^{LM}$ (and its transpose $\mathbf{R}_2^{ML}$) representing the intermolecular cross-relaxation rate. The $\mathbf{R}_2^{L}$ and $\mathbf{R}_2^{M}$ also contain diagonal terms associated with the intermolecular relaxation. The *generalized* kinetic matrix **K** is given by [14]:

$$\mathbf{K} = \begin{bmatrix} \mathbf{K}_{12} & -\mathbf{K}_{21} \\ -\mathbf{K}_{12} & \mathbf{K}_{21} \end{bmatrix} \tag{3}$$

where

$$\mathbf{K}_{12} = \begin{bmatrix} \mathbf{k}_{12}^{L} & 0 \\ 0 & \mathbf{k}_{12}^{M} \end{bmatrix} \quad \text{and} \quad \mathbf{K}_{21} = \begin{bmatrix} \mathbf{k}_{21}^{L} & 0 \\ 0 & \mathbf{k}_{21}^{M} \end{bmatrix} \tag{4}$$

Here $\mathbf{k}_{12}^{L} = k_{on}[M_1]\ \mathbf{1}_L$, $\mathbf{k}_{12}^{M} = k_{on}[L_1]\ \mathbf{1}_M$, $\mathbf{k}_{21}^{L} = k_{off}\ \mathbf{1}_L$ and $\mathbf{k}_{21}^{M} = k_{off}\ \mathbf{1}_M$. The dimensions of the unit matrices depend on the species indicated by the subscript (ligand or macromolecule).

We have also developed a three-state model [14] to describe the binding of a ligand to a receptor that undergoes hinge-bending (with the active site being formed in the closed state only, see Fig. 2). In this model ($L_1 + M_1 \rightleftarrows L_2M_2 \rightleftarrows L_3M_3$), state (1) consists of free ligand and free macromolecule. States (2) (L_2M_2) and (3) (L_3M_3) correspond to the open and closed forms of the ligand–receptor complex. The *generalized* relaxation rate matrix **R** for this case is [14]

$$\mathbf{R} = \begin{bmatrix} \mathbf{R}_1 & 0 & 0 \\ 0 & \mathbf{R}_2 & 0 \\ 0 & 0 & \mathbf{R}_3 \end{bmatrix} \tag{5}$$

The $\mathbf{R}_2$ and $\mathbf{R}_3$ matrices have definitions similar to $\mathbf{R}_2$ in

a

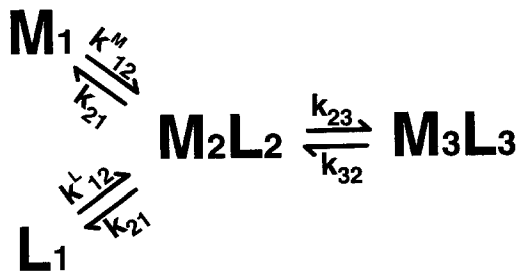

b

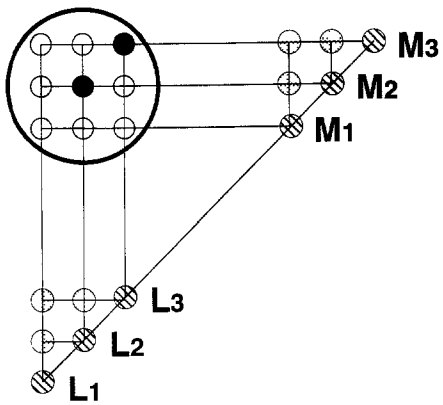

Fig. 2. (a) Kinetic scheme for a three-state model of a ligand binding to a macromolecule with hinge-bending motion. Here the free state is designated as (1), the intermediate state (with ligand bound to the enzyme with the active site in the open state) as (2), and the productive state (with ligand bound in the closed active site) as (3). The hinge-closing and opening rates are k_{23} and k_{32}, respectively. (b) Schematic for the NOESY spectrum for a three-state model description of a ligand–receptor complex. The small circles have the same significance as in the two-state model (Fig. 1).

Eq. 2, and correspond to the open and closed states of the complex, respectively.

The generalized exchange matrix **K** is [14]

$$\mathbf{K} = \begin{bmatrix} \mathbf{K}_{12} & -\mathbf{K}_{21} & 0 \\ -\mathbf{K}_{12} & (\mathbf{K}_{21}+\mathbf{K}_{23}) & -\mathbf{K}_{32} \\ 0 & -\mathbf{K}_{23} & \mathbf{K}_{32} \end{bmatrix} \qquad (6)$$

where

$$\mathbf{K}_{23} = \begin{bmatrix} \mathbf{k}_{23}^{L} & 0 \\ 0 & \mathbf{k}_{23}^{M} \end{bmatrix} \quad \text{and} \quad \mathbf{K}_{32} = \begin{bmatrix} \mathbf{k}_{32}^{L} & 0 \\ 0 & \mathbf{k}_{32}^{M} \end{bmatrix} \qquad (7)$$

$\mathbf{k}_{23}^{n} = k_{23}^{n}\ \mathbf{1}_n$ and $\mathbf{k}_{32}^{n} = k_{32}^{n}\ \mathbf{1}_n$, where k_{23}^{n} and k_{32}^{n} are the hinge-bending rates (n is either L or M). For the hinge-bending motion case considered here, we assume that $k_{23}^{L} = k_{23}^{M}$ and $k_{32}^{L} = k_{32}^{M}$. We obtain a general solution for the NOESY intensities of the total system from the equation [4,14]

$$\mathbf{I} = \mathbf{U} \exp\{-\Lambda\tau\}\ \mathbf{U}^{-1}\ \mathbf{I}(0) \qquad (8)$$

where **U** is a transformation matrix which diagonalizes the dynamic matrix [**R** + **K**],

$$\mathbf{U}^{-1}\ [\mathbf{R}+\mathbf{K}]\ \mathbf{U} = \Lambda \qquad (9)$$

and **I**(0) is a matrix with elements proportional to the concentrations of the various species [14]. For computational purposes, the asymmetric matrix **R** + **K** can be transformed to a symmetric form [5,14] and diagonalized for any arbitrary set of exchange rates.

In even the simplest two-state models of an inter-TrNOESY experiment, a total of *ten categories of resonances* arise from combinations of cross-relaxation and exchange events (Fig. 1b). This is because four species are involved in this model (free ligand, bound ligand, free macromolecule, and bound macromolecule). Four of the ten categories represent intramolecular NOESY spectra for the four species. Two categories refer to exchange cross-peaks between the free and bound forms of the ligand and receptor. Each of these include both direct-exchange peaks and exchange-mediated intra-TrNOESY peaks between the free and bound states of a particular molecule [4,26]. The remaining four categories represent *intermolecular* NOESY peaks between dissimilar molecules (i.e., between a ligand and a receptor) in their free and bound states. These *inter*-TrNOESY peaks are grouped together in Fig. 1b by a large circle. One of these is dominated by direct-dipolar cross-relaxation in the complex (filled circle), and the other three by exchange-mediated interactions (open circles, vide infra). In a similar manner, a three-state model of a ligand–receptor interaction can result in a total of 21 categories of peaks (see Fig. 2). The CORCEMA program is capable of calculating intensities for all possible resonances in an N-state model of a transferred NOESY experiment. Individual resonances within any single category can only be observed when the exchange is slow on the chemical-shift scale. When the exchange is fast on the chemical-shift scale, the components of an individual inter-TrNOESY interaction will collapse together, resulting in a single peak. The intensity of that peak is the sum of the components. Expressions for the compressed NOESY intensity matrix, when the exchange is fast on the relaxation and chemical-shift scales, are given in the Appendix for the two- and three-state models.

Methods

To examine the factors that influence the inter-TrNOESY, we performed calculations for two model systems by solving the general equation (Eq. 8) *valid for all exchange rates*, using the CORCEMA algorithm described previously [14]. First, we simulated several aspects of the behavior of the inter-TrNOESY for a hypothetical two-state model derived from the published data on a

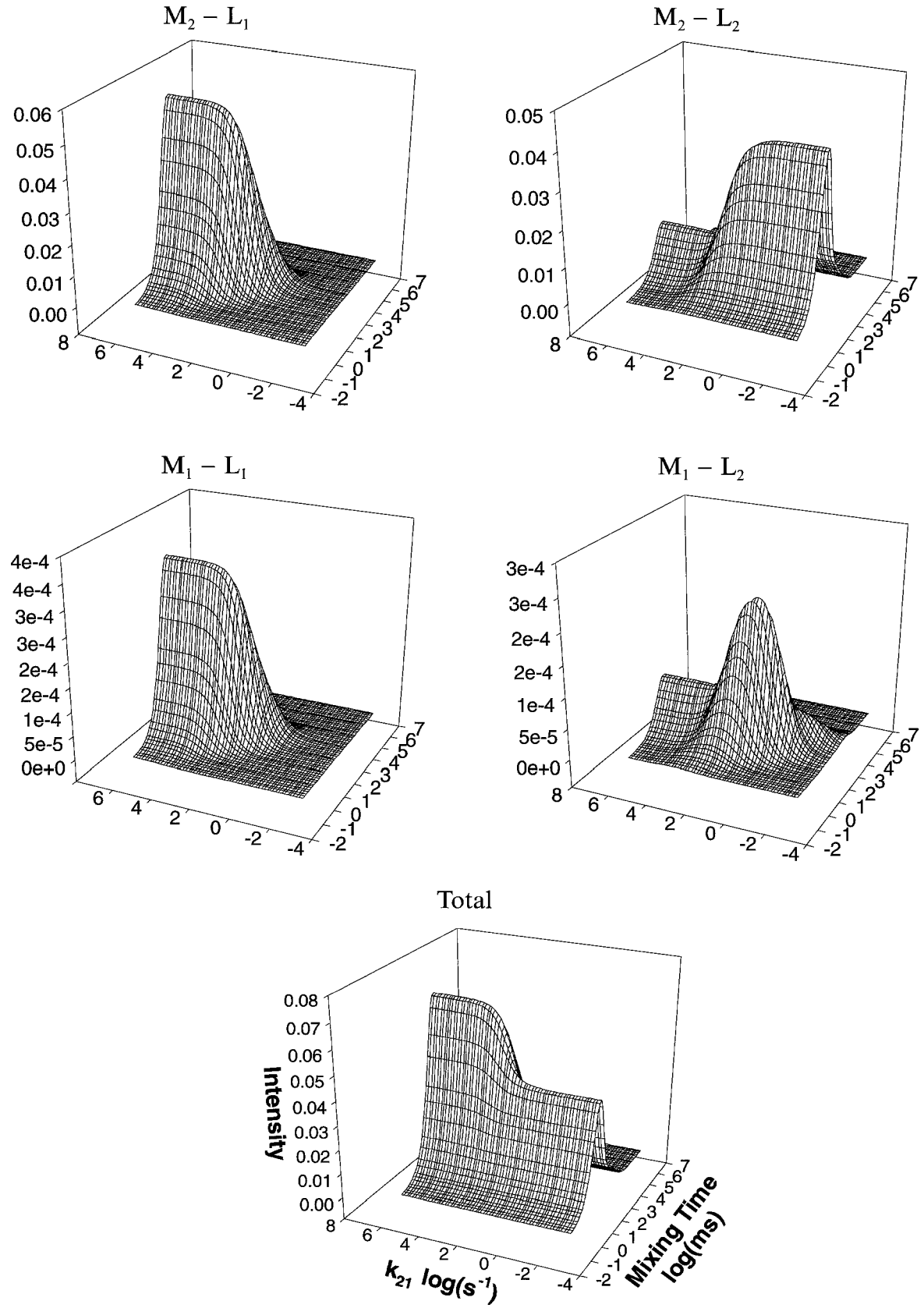

Fig. 3. Effect of enzyme off-rate (k_{21}) and mixing time on the inter-TrNOESY between the Trp^{177} ε3(H) and γ1(CH_3) protons (effective distance 2.6 Å) in a neuraminidase–BANA complex. BANA is 4-acetamido-3-guanidinobenzoic acid. The four individual components described in the text (see Fig. 1b) and their sum are shown.

neuraminidase complex [27] with a benzoic acid analogue of *N*-acetylneuraminic acid (BANA), bound in the active site. We included the coordinates of 12 residues constituting the *first shell* of the active site in the protein (Arg^{116}, Glu^{117}, Asp^{149}, Arg^{150}, Trp^{177}, Arg^{223}, Glu^{226}, Glu^{275}, Glu^{276}, Arg^{292}, Arg^{374}, His^{409}) and BANA, bound in the active site, in these calculations. To illustrate the potential of the CORCEMA program to perform realistic model calculations, we focus on interactions between the γl methyl group on the ligand and the ring protons from Trp^{177} on the enzyme. Other conditions for the simulations were a ligand-to-enzyme ratio of 5 :1 unless otherwise stated, with a total ligand concentration [L_t] of 1 mM, a dissociation constant K_D of 5×10^{-6} M, rotational correlation times (τ_c) of 50 ns for both the complex and the free protein, and of 0.3 ns for the free ligand (corresponding to null NOE at 600 MHz), an internal correlation time of 10^{-13} s for the methyl groups, and a leakage factor of 0.2 s^{-1} for the protein and ligand. In Fig. 3, the effective distance between the γl(CH_3) protons on the ligand and the Trp^{177} ε(H) proton on the enzyme is 2.6 Å. This is defined as $\{1/3\,\Sigma r^{-3}\}^{-1/3}$, where r is the distance from each individual methyl proton to the ε(H) proton. In Fig. 4, we examine the direct and indirect effects of variations in proton–proton distances on the inter-TrNOESY. To model the influence of *second-shell* residues on the intensities, we added the residue Ala^{200} to the second shell of the active site such that Trp^{177} (in the first shell) is between the ligand and Ala^{200}. In Fig. 4a, the Ala^{200} methyl protons are effectively 6.5 Å from the Trp^{177} η2 proton and 9.7 Å from the ligand methyl group. In Fig. 4b the backbone torsion angles of this residue were changed to make these distances 3.2 Å from the Trp^{177} η2 proton and 6.58 Å from the ligand methyl group. In both figures, the effective distances between the three γl methyl protons on the ligand and the ζ3, η2 and ζ2 protons on the protein Trp^{177} residue are 2.6, 4.8 and 6.5 Å, respectively. In these calculations, we assumed that the rates of association and dissociation were fast on the relaxation rate scale ($k_{on} = 10^9\ s^{-1}\ M^{-1}$, $k_{21} = 5 \times 10^3\ s^{-1}$). Bound water molecules in the crystal structure were omitted, which is equivalent to performing these NMR measurements in D_2O. For waters with long residence times, their effect can be simulated (in a presaturation or a jump-return NOESY spectrum) by including additional leakage factors for protein and ligand protons in the vicinity of the water molecules. For simplicity, we assumed that the ligand conformation did not change upon binding. We normalized all intensities with respect to the total diagonal intensity of a single ligand proton (i.e. free + bound) at zero mixing time.

Lastly, we present an analysis of the influence of motions within the macromolecule on the magnitude of the inter-TrNOESY. To do this, we performed calculations for a hypothetical three-state model of a thermolysin/leucine-inhibitor complex. Our model is similar to that used in our previous work on the intra-TrNOESY [11–14] and is loosely based on a model proposed from crystallo-

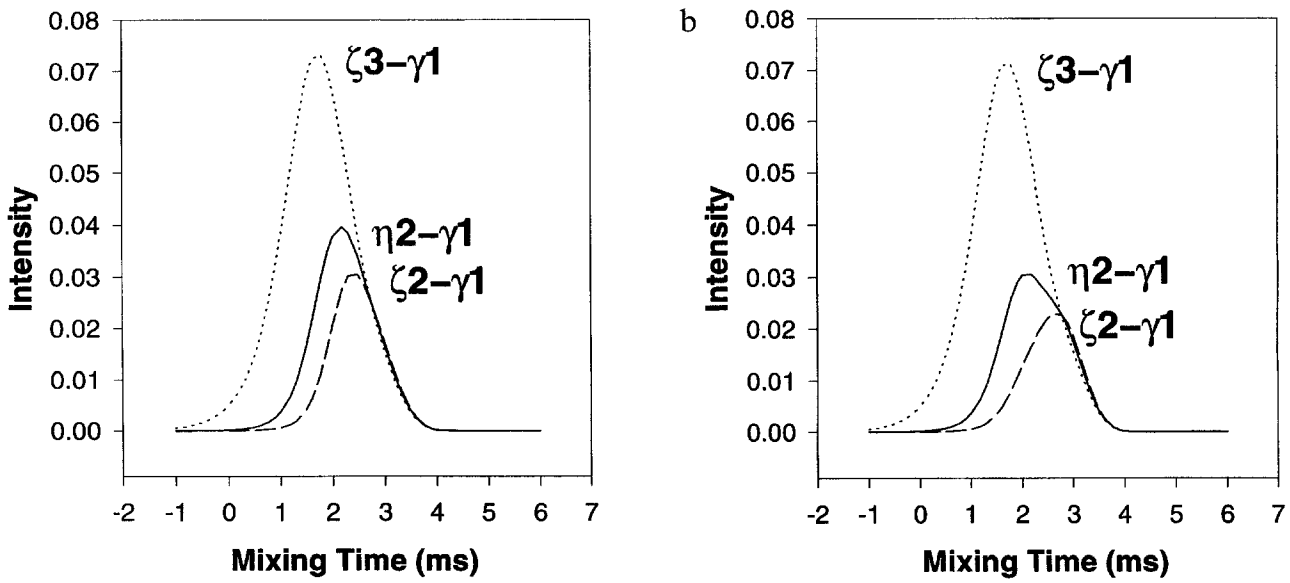

Fig. 4. Distance dependence of inter-TrNOESY intensities for a neuraminidase–BANA complex. The plots represent intermolecular contacts between γl(CH_3) on the ligand and Trp^{177} ring protons on the enzyme: Trp^{177} ζ3(H)–γl(CH_3) (2.6 Å, ····); Trp^{177} η2(H)–γl(CH_3) (4.8 Å, —); and Trp^{177} ζ2(H)–γl(CH_3) (6.5 Å, – –). The first shell in the active site consists of 12 residues (mentioned in the text). Only Ala^{200} is included in the second shell, for computational purposes. In (a), the Ala^{200} methyl group is 9.7 Å from γl(CH_3) and 6.5 Å from Trp^{177} η2(H). In (b), these distances are 6.6 and 3.2 Å, respectively. A comparison of the intensities in (a) and (b) demonstrates the effect of second-shell residues on the inter-TrNOESY with first-shell residues, during the later phases of the NOESY growth curves. Note that the mixing time is shown in a logarithmic scale.

graphy [28]. We included active-site residues Asn^{112}, Ala^{113}, Phe^{114}, Trp^{115}, Asn^{116}, Glu^{143}, His^{146}, Arg^{203} and His^{231}, and a leucine-based inhibitor (CH_3CO(N-OH)Leu-OCH_3) in the model. We calculate the results for interactions between the m1 methyl group (acetyl group) on the ligand and the Ala^{113} methyl group on the protein. In the closed state, the effective distance between these groups is 3.6 Å. In the open state, however, the distance is assumed to increase to 5.4 Å. We assumed a dissociation constant K_D of 1.8×10^{-4} M, a mixing time of 800 ms, and a relatively high ligand/enzyme ratio of 20 :1 with $[L_t] = 0.002$ M. Other factors, such as correlation times and leakage rates, are the same as for the neuraminidase complex. A scheme for this three-state model is shown in Fig. 2.

Results

First we present the results for a two-state model of BANA–neuraminidase interactions. Figure 3 illustrates how the four components and the total sum of the inter-TrNOESY intensities vary as a function of the off-rate k_{21} (the dissociation rate of the complex) and the NOESY mixing time τ, for the contact between the neuraminidase Trp^{177} ε3(H) and BANA γ1(CH_3) protons. These four individual components (shown enclosed in a large circle in Fig. 1) are observable only if the conformational exchange is slow on the chemical-shift scale. The intensity surface labeled M_2–L_2 describes the direct NOESY cross-peak between the bound ligand and bound protein (filled circle in Fig. 1b). As one can see from the figure, this surface dominates when the exchange rate is slow, but is not a major contributor when the exchange rate is fast (compared to the cross-relaxation rate). The M_1–L_1 intensity surface contributes little to the total intensity because there is so little free macromolecule. The intensity surfaces labeled M_1–L_2 and M_2–L_1 describe exchange-mediated NOESY cross-peaks between bound and free species due to a single exchange process. The latter surface dominates the total sum intensity surface under conditions of fast exchange because there is more bound macromolecule and the free ligand is in excess. The surfaces M_1–L_1 and M_1–L_2 have very small intensity because they describe effects mediated by free protein and there is little free protein available when the ligand is in excess.

To investigate the sensitivity of inter-TrNOESY spectra to variations in proton–proton distances (short, medium and long range) between the ligand and active-site residues, and to study the effect of second-shell residues surrounding the active site, we performed CORCEMA calculations using our neuraminidase–BANA model. Both Figs. 4a and b show intensity variations for the same three interactions between a γ1 methyl group on the ligand and three Trp^{177} protons (ζ3, η2, ζ2) on the protein. In Fig. 4b, however, the second-shell Ala^{200} is positioned closer to Trp^{177} than in Fig. 4a. Parameters for these calculations are given in the Methods section.

We calculated the effect of the dissociation constant K_D on the magnitudes of inter-TrNOESY between the Trp^{177} ε3(H) and γ1(CH_3) protons of our neuraminidase–BANA model. We assumed that the association rate of the ligand was essentially diffusion-limited ($k_{on} = 10^9$ s^{-1} M^{-1}) so that the dissociation constant K_D not only determines the fraction of bound ligand, but also controls the rate of dissociation, since $k_{21} = K_D\, k_{on}$. Figure 5 shows the results. We also examined the effect of varying the $[L_t]/[M_t]$ ratio on the same inter-TrNOESY interaction in the neuraminidase complex. We varied $[M_t]$ but fixed $[L_t]$ at 10 mM, K_D at 5×10^{-6} M, and k_{on} at 10^9 s^{-1} M^{-1}. Figure 6 shows the results for these calculations.

To illustrate the full potential of the CORCEMA program, we created a more complex model system based on a number of studies that indicate that some enzymes undergo motions upon binding a substrate [28–31]. To characterize the effects of these motions on the inter-TrNOESY intensities, we developed a three-state model of thermolysin, undergoing hinge-bending upon binding a leucine-based inhibitor, as described in the Methods section. We computed the inter-TrNOESY for the interaction between the m1 methyl on the ligand and the Ala^{113} methyl on the enzyme as a function of the dissociation rate (k_{21}) and the hinge-bending rate (k_{23}). The total intensity surface shown in Fig. 7 was derived from a series of CORCEMA calculations whereby k_{21} and k_{23} were varied incrementally.

Discussion

The results of our calculations show that the behavior of the inter-TrNOESY is actually somewhat different from that of intra-TrNOESY. This is dramatically reflected in the different dependences on $[L_t]/[M_t]$ for inter-NOESY (Fig. 6) and intra-TrNOESY (Fig. 6 in Ref. 14). The former strictly arises from the dipolar relaxation within the complex and hence has the same sign as the protein NOESY. Further, the intensity maxima appear at shorter mixing times, as in a larger protein. The intra-TrNOESY, on the other hand, is influenced by the dipolar relaxation in the free ligand as well, and hence its sign depends on the $[L_t]/[M_t]$ ratio (being negative for very large values of the ratio where the relaxation is dominated by that of the free ligand, and positive for moderately large ratios when the bound ligand makes a dominant contribution). Further, the intensity maxima shift dramatically depending on $[L_t]/[M_t]$.

The four individual components of the total inter-TrNOESY intensity presented in Figure 3 can be observed individually only if the exchange is slow on the chemical-shift scale (as in the case of Trp binding reversibly to the 37 kDa Trp-repressor/operator complex [32]).

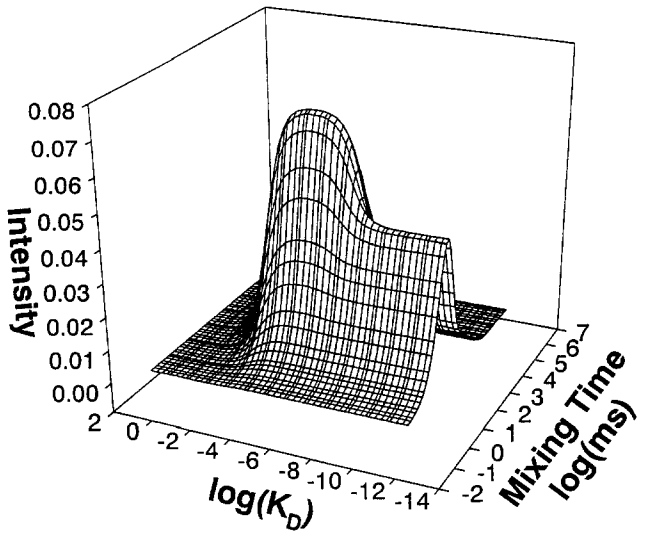

Fig. 5. Effect of dissociation constant (K_D) on the inter-TrNOESY between the Trp^{177} ε3(H) and γ1(CH_3) protons in a neuraminidase–BANA complex.

In the extreme of this limit (i.e., for a tight binding complex where the exchange rate is too slow compared to the relaxation rate as well), the only significant contribution to the inter-TrNOESY is from the direct transfer of magnetization between the two bound species (M_2–L_2), and this interaction is more aptly described as a NOESY. At the other extreme, when the conformational exchange is very fast on the chemical-shift scale, only a single set of intensities is observed which is a sum total of the four components. In this limit, the most significant contribution comes from the exchange-mediated transfer of magnetization between the bound enzyme and the free ligand (M_2–L_1), when the ligand is in excess. If the exchange rate is intermediate on the chemical-shift scale, line-broadening problems [33] may make it difficult to quantitatively measure the total intensity under poor signal/noise conditions.

The surface labeled M_1–L_1 does not arise from a direct dipolar interaction between the free species. Instead, it describes the development of a pseudo-direct NOESY peak according to the the following scheme for magnetization transfer between the free molecules:

$$\underset{L_1}{} \overset{\text{exchange}}{\cdots\cdots} \underset{L_2}{} \overset{\text{dipolar}}{\longleftrightarrow} \underset{M_2}{} \overset{\text{exchange}}{\cdots\cdots} \underset{M_1}{}$$

Even though there is *no direct cross-relaxation* between L_1 and M_1, as the exchange rates gradually increase (i.e., the on- and off-rates in Fig. 1a, an exchange-mediated NOESY peak between L_1 and M_1 develops through the double-exchange process shown above. Single- and double-exchange-mediated cross-peaks have been described in detail by our laboratory [4,26].

The intensities of the three inter-TrNOESY contacts in Fig. 4a or b for the fast exchange condition show significant differences that reflect the variations in the intermolecular distances between the ligand γ1 methyl group and the Trp^{177} ring protons. These results suggest that a ligand can be docked in the first shell of the active site of a macromolecule at least semiquantitatively, using a distance geometry/dynamical-simulated-annealing refinement [34], together with strong-medium-weak type of restraint criteria for the inter-TrNOESY contacts (vide infra). A comparison of the corresponding NOESY curves between Figs. 4a and b also shows some significant differences. The major difference in the simulation conditions in Figs. 4a and b is the orientation of Ala^{200} in the second shell of the active site – the Ala^{200} methyl is farther from Trp^{177} in (a) and closer in (b). In both cases, Ala^{200} is sufficiently far from the bound ligand γ1 methyl group (distances of 9.7 and 6.58 Å, respectively, in Figs. 4a and b) that no *direct* intermolecular NOESY contact is possible between them. By comparing the two figures, the following conclusions can be drawn: (i) The *initial* portions of the growth curve remain invariant in both the figures. In this regime, the intensities are dominated by dipolar contacts with residues in the first shell of the active site; (ii) For longer times during the growth phase of the NOESY intensities, however, significant differences are observed in Figs. 4a and 4b. At these mixing times, residues in the second shell of the active site begin to contribute to the inter-TrNOESY intensities of the first-shell residues due to spin diffusion. Note that these contributions from the second shell are especially felt by long-range (i.e., weak intensities) contacts with protons in the first shell. Both these observations are predicted by Eq. A4. It can be shown that similar results are obtained for intra-

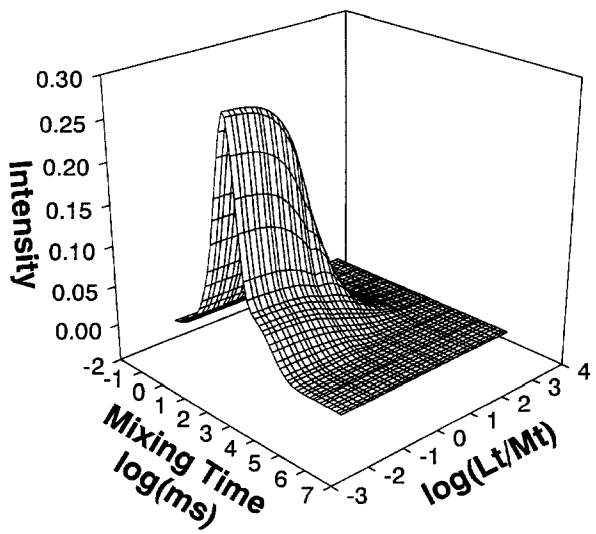

Fig. 6. Effect of varying ligand/enzyme ratio (L_t/M_t) on the inter-TrNOESY between the Trp^{177} ε3(H) and γ1(CH_3) protons in a neuraminidase–BANA complex.

TrNOESY as well, if ligand–receptor intermolecular relaxation is significant (Eq. A5). These results suggest that even when the receptor NOESY spectrum is not experimentally observable, both intraligand TrNOESY and inter-TrNOESY can potentially serve as experimental constraints on the relative orientation of the first- and second-shell residues in the active site (vide infra). A starting conformation for these residues may be obtained from known crystallographic structures, when available.

The results presented in Fig. 5 show that there is a small range of K_D values between 10^{-4} and 10^{-7} M which marks the optimum range for observing the inter-TrNOESY effect. For $K_D < 10^{-8}$ M (tight binding complexes), the inter-TrNOESY is essentially constant because the lifetime of the complex is much longer than the intermolecular cross-relaxation time. As K_D becomes larger than 10^{-7} M, the inter-TrNOESY is enhanced first (due to increasing intensity of the exchange-mediated cross-peak M_2–L_1), and reaches a plateau between 10^{-6} and 10^{-4} M. For even larger values of K_D (>10^{-4} M), the effect drops off very rapidly since the binding is too weak to form a complex with any significant population. The NOESY spectra of tight binding complexes (such as calmodulin complexes with myelin basic protein fragment [35]) fall on the short value range ($K_D < 10^{-8}$ M) in the figure, where the intensities are independent of exchange. They are relatively straightforward to analyze for structural calculations, and do not necessitate the use of the CORCEMA algorithm even though it is capable of analyzing the data in the whole range.

The effect of varying $[M_t]$ on the inter-TrNOESY (while holding $[L_t]$ constant) is examined in Fig. 6. It is seen that the intensity steadily increases as $[L_t]/[M_t]$ decreases, and reaches a plateau for ratios < 1 since all the ligand is bound at this limit. These calculations confirm experimental observations made several years ago [16]. We have previously shown that high $[L_t]/[M_t]$ values (e.g., 20:1 or greater) tend to favor protein-mediated spin-diffusion pathways over ligand-mediated pathways in intraligand TrNOESY measurements, and have suggested the use of somewhat lower ratios to restore to the experiment its sensitivity to ligand-mediated pathways [11–14]. According to the results in Fig. 6, these lower $[L_t]/[M_t]$ ratios also result in a significant build-up of inter-TrNOESY intensities, which can be exploited in structural refinements.

Motions in the complex (i.e., fast side-chain motions or slow hinge-bending motions) can also have a dramatic effect on the inter-TrNOESY intensities; hence, these motions need to be taken into account in a quantitative analysis of the intensities. This holds true even for tight binding complexes which undergo significant motions in the active site. The results of Fig. 7 show that even when the off-rate of the ligand is slow, the inter-TrNOESY intensity is still influenced by the hinge-closing rate. The

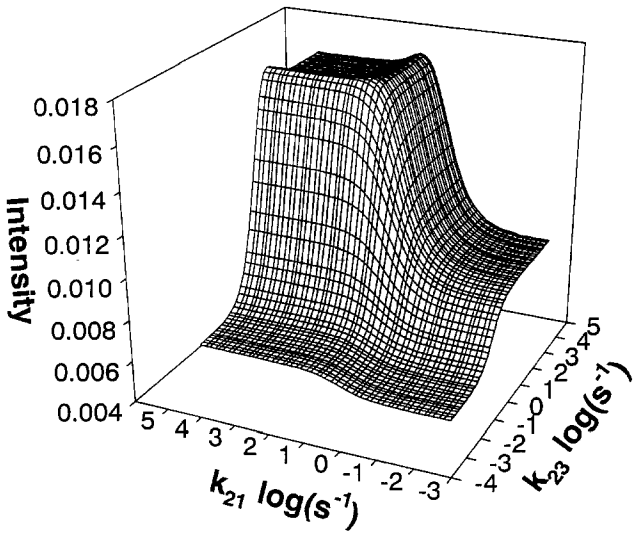

Fig. 7. Intensity profile for the inter-TrNOESY contact between $Ala^{133}(CH_3)$ on thermolysin and m1(CH_3) on a leucine inhibitor as a function of k_{21} (off-rate) and k_{23} (hinge-bending rate). The mixing time used was 800 ms. The intensity profile surface is the sum of nine contributions, consisting of a pseudo-direct (L_1–M_1), and two direct (L_2–M_2, L_3–M_3) and six exchange-mediated intermolecular NOESY peaks (L_1–M_2, L_1–M_3, L_2–M_1, L_2–M_3, L_3–M_1 and L_3–M_2). These are defined in Fig. 2.

four plateau regions on the intensity surface correspond to the four exchange regimes, where the rates k_{21} and k_{23} are either fast or slow in comparison to the cross-relaxation rate. Ridges at the top plateau indicate that the intensity maximum is still shifting toward shorter mixing times as k_{21} and k_{23} increase. This and the other effects of motions in the active site require careful analysis, but may be important in studies of enzyme mechanisms. The CORCEMA algorithm provides a convenient framework for such analysis. When the exchange rate is very fast on the relaxation rate scale, the intensities become independent of the exchange rates, and the analysis of the intra- and inter-TrNOESY is simpler [14].

The experimental observation of inter-TrNOESY contacts between a ligand and a large macromolecule by a number of investigators [15–23,32] establishes that a quantitative measurement of these intensities is indeed possible for small to moderate-sized complexes. Anglister and co-workers [21] have successfully identified inter-TrNOESY contacts between an antibody/antigen complex using difference-NOESY methods as well as a perdeuterated antibody. A spin-echo filtered NOESY technique was successfully employed to identify intermolecular contacts of a ligand with Fab [23]. Arrowsmith and co-workers [32] used ^{13}C-edited NOESY to identify (and assign) *all intermolecular contacts* between a reversibly bound labeled tryptophan and a repressor/operator complex (~37 kDa).

The many limitations associated with NOESY structural studies of high-molecular-weight proteins (≥40 kDa)

also apply to the inter-TrNOESY. In principle at least, the complete TrNOESY spectrum (i.e., intraligand, intrareceptor, and intermolecular) can be characterized and assigned for smaller molecular weight complexes (< 20–25 kDa). Uniform ^{15}N and ^{13}C labeling together with isotope edited/filtered methods and multidimensional NMR analysis [35–37] facilitates a complete characterization of these smaller complexes. Interestingly, such methods have been successfully used to identify intermolecular NOESY contacts of a labeled tryptophan that *reversibly binds* to a 37 kDa operator/repressor complex [32]. For proteins larger than ~25 kDa, where dipolar broadening and spin-diffusion problems can potentially hinder the analysis of the receptor NOESY spectrum, one has to resort to alternative methods. For macromolecules up to about 40 kDa, random fractional deuteration or reverse protonation of active-site residues in an otherwise completely deuterated receptor may help somewhat alleviate line-broadening and spin-diffusion problems [38]. In this situation, isotope filtered/edited methods may facilitate assignment of the inter-TrNOESY contacts between the ligand and the active-site residues.

There are four different refinement methods that could be used to deduce the ligand–receptor (active-site) conformation. We briefly summarize them below:

(i) Using a known or an approximate conformation for the active site (e.g., from crystallography), one could dock the ligand within the active site using experimental inter-TrNOESY contacts semiquantitatively as distance constraints according to strong-medium-weak type of criteria, in a distance geometry/dynamical-simulated-annealing procedure [34]. This procedure exploits the sensitivity of inter-TrNOESY to intermolecular proton–proton distances in the active site (see Fig. 4a). All the protons on the ligand and on the active-site residues could be included in this refinement. The crystal structure is also useful in making the intermolecular NOESY assignments. If the crystal structure for a protein of interest is not available, an approximate starting conformation of the active site can be modeled from the known structures of homologous proteins by molecular replacement methods.

(ii) A second approach involves proposing several alternative models [39] for the complex, and predicting both intraligand and inter-TrNOESY intensities using CORCEMA. In the current version of the CORCEMA program, for a given proposed model of the ligand–receptor complex, the algorithm computes inter-TrNOESY as well as intra-NOESY spectra, which can be compared with experimental data using NOE R-factors [39]. If the agreement is not satisfactory, alternative models for the complex could be proposed, and the model that gives the best fit can be identified [39]. If the intrareceptor NOESY spectra are observed experimentally, these data can be included in this procedure as well.

(iii) Alternatively, the CORCEMA program can be adapted for direct methods that use a back-transformation of an experimental intensity matrix into a relaxation rate matrix [40–42]. In the present case, this will be a back-transformation to an average relaxation rate matrix $\langle \mathbf{R} \rangle$ for fast exchange (see the Appendix) or into the sum matrix $\mathbf{R} + \mathbf{K}$ for the general case. A hybrid-matrix approach [40–42] could further extend the utility of the direct method under conditions where not all of the intensities can be measured accurately (e.g., the intrareceptor NOESY contacts in large complexes). In the hybrid-based refinement protocol, one augments the experimental NOESY spectrum with calculated NOESY intensities for those peaks that cannot be measured (e.g., the intra-NOESY intensities for the receptor). Relaxation and exchange matrices would be back-calculated from the NOE matrix with distances being derived from the relaxation matrix. These distances would then be used as restraints for building a new model.

(iv) Yet another alternative is to use intensity-based refinement procedures [43–49] to iteratively optimize a target function consisting of *experimentally measurable intensities* only (e.g., intraligand TrNOESY and inter-TrNOESY). The target function can be constructed to be simple [48,49] or variable [43–45]. The optimization can be efficiently performed either with least-squares refinement [49], numerical or analytical gradient-based intensity-restrained refinement [43–45,48] or simulated-annealing-based methods [46,47], or a combination of these. These procedures typically use data at several mixing times during the growth phase of the NOESY intensity curves where spin diffusion from unobservable protons (e.g., active-site residues of an enzyme) also can influence the observable intensities, and hence are amenable to refinement *to some extent*. Recent experimental work from our laboratory has confirmed this prediction [44]. As inferred from Eq. 2, A4 and A5, a rigorous characterization of the ligand–receptor complex requires a knowledge of the relaxation rate matrix $\mathbf{R}_2^M$ for the macromolecule (active-site residues). Even if the intra-NOESY spectra for the active-site residues are not amenable for direct observation, because the intraligand TrNOESY (Eq. A5) and the inter-TrNOESY (Eq. A4) both depend upon the R_2^M matrix, they have the potential to serve as experimental constraints in the refinement of the active-site conformation. This is confirmed by the results in Figs. 4a and b.

In these refinements, it is helpful to take into account external leakage factors as accurately as possible to calculate the intensity profiles, even though their effect is not significant during the growth phase of the intensities. Some typical leakage factors arise due to weak interactions with paramagnetic oxygen in solution, exchange of amide protons with bulk solvent, and dipolar interaction of amide hydrogens with quadrupolar nitrogen [39].

Conclusions

Using simulations based on CORCEMA theory, we have examined the dependence of inter-TrNOESY on a number of factors. Our results underscore the potential of this technique in developing quantitative models of ligand–receptor complexes for use in rational drug design. Together with these approaches and the CORCEMA theory, the inter-TrNOESY, whenever observable, is likely to contribute toward an improved structure-based design of ligands (or drugs) because now the active-site residues can be explicitly incorporated in a quantitative structure refinement protocol.

Acknowledgements

This work was supported by grant MCB-9118503 from the National Science Foundation, and by grants CA-13148 and CA-38587 from the National Institutes of Health. The coordinates for the BANA–neuraminidase complex were kindly provided by Dr. Ming Luo.

References

1 Clore, G.M. and Gronenborn, A.M., J. Magn. Reson., 48 (1982) 402.
2 Clore, G.M. and Gronenborn, A.M., J. Magn. Reson., 53 (1983) 423.
3 Ni, F., Prog. NMR Spectrosc., 26 (1994) 517.
4 Lee, W. and Krishna, N.R., J. Magn. Reson., 98 (1992) 36.
5 Ni, F., J. Magn. Reson., 96 (1992) 651.
6 London, R.E., Perlman, M.E. and Davis, D.G., J. Magn. Reson., 97 (1992) 79.
7 Lippens, G.M., Cerf, C. and Hallenga, K., J. Magn. Reson., 99 (1992) 268.
8 Zheng, J. and Post, C.B., J. Magn. Reson., B101 (1993) 262.
9 Lian, L.Y., Barsokov, I.L., Sutcliffe, M.J., Sze, K.H. and Roberts, G.C.K., Methods Enzymol., 239 (1994) 657.
10 Ni, F. and Zhu, Y., J. Magn. Reson., B103 (1994) 180.
11 Jackson, P.L., Moseley, H.N.B. and Krishna, N.R., J. Magn. Reson., B107 (1995) 289.
12 Moseley, H.N.B., Curto, E.V. and Krishna, N.R., Proceedings of the 35th Experimental NMR Conference, Asilomar, CA, U.S.A., 1994, WP115.
13 Moseley, H.N.B., Curto, E.V. and Krishna, N.R., International Symposium on NMR as a Structural Tool for Macromolecules, Indianapolis, IN, U.S.A., 1994.
14 Moseley, H.N.B., Curto, E.V. and Krishna, N.R., J. Magn. Reson., B108 (1995) 243.
15 Balaram, P., Bothner-By, A.A. and Breslow, E., J. Am. Chem. Soc., 94 (1972) 417.
16 James, T.L., Biochemistry, 15 (1976) 4724.
17 Vasak, M., Nagoyama, K., Wüthrich, K., Mertens, M.L. and Kagi, J.H.R., Biochemistry, 18 (1979) 5050.
18 Fry, D.C., Kuby, S.A. and Mildvan, A.S., Biochemistry, 24 (1985) 4680.
19 Ferrin, L.F. and Mildvan, A.S., Biochemistry, 24 (1985) 6904.
20 Anglister, J. and Zilber, B., Biochemistry, 29 (1990) 921.
21 Anglister, J., Scherf, T., Zilber, B., Levy, R., Zvi, A., Hiller, R. and Feigelson, D., Faseb J., 7 (1993) 1154.
22 Plesniak, L.A., Boegemann, S.C., Segelke, B.W. and Dennis, E.A., Biochemistry, 32 (1993) 5009.
23 Arepalli, R.S., Glaudemans, C.P.J., Daves Jr., G.D., Kovac, P. and Bax, A., J. Magn. Reson., B106 (1995) 195.
24 Scherf, T. and Anglister, J., Biophys. J., 64 (1993) 754.
25 Krishna, N.R., Goldstein, G. and Glickson, J.D., Biopolymers, 19 (1980) 2003.
26 Choe, B.Y., Cook, G.W. and Krishna, N.R., J. Magn. Reson., 94 (1991) 387.
27 Janakiraman, M.N., White, C.L., Laver, W.G., Air, G.M. and Luo, M., Biochemistry, 33 (1994) 8172.
28 Holland, D.R., Tronrud, D.E., Pley, H.W., Flaherty, K.M., Stark, W., Jansonius, J.N., McKay, D.B. and Matthews, B.W., Biochemistry, 31 (1992) 11310.
29 Quiocho, F.A., Curr. Opin. Struct. Biol., 1 (1991) 922.
30 Lumb, K.J., Cheetan, J.C. and Dobson, C.M., J. Mol. Biol., 235 (1994) 1072.
31 Radmacher, M., Fritz, M., Hansma, H.G. and Hansma, P.K., Science, 265 (1994) 1577.
32 Lee, W., Revington, M., Farrow, N.A., Nakamura, A., Utsunomiya-Tate, N., Miyake, Y., Kainosho, M. and Arrowsmith, C.H., J. Biomol. NMR, 5 (1995) 367.
33 Ni, F., J. Magn. Reson., B106 (1995) 147.
34 Nilges, M., Clore, G.M. and Gronenborn, A.M., FEBS Lett., 239 (1988) 129.
35 Ikura, M., Clore, G.M., Gronenborn, A.M., Zhu, G. and Bax, A., Science, 256 (1992) 632.
36 Wider, G., Weber, C., Traber, H., Widmer, H. and Wüthrich, K., J. Am. Chem. Soc., 112 (1990) 9015.
37 Gemmecker, G., Olejniczak, E.T. and Fesik, S.W., J. Magn. Reson., 96 (1992) 199.
38 a. LeMaster, D.M., Methods Enzymol., 177 (1989) 23.
b. Nietlispach, D., Clowes, R.T., Broadhurst, R.W., Ito, Y., Keeler, J., Kelly, M., Ashurst, J., Oschkinat, H., Domaille, P.J. and Lave, E.D., J. Am. Chem. Soc., 118 (1996) 407.
39 Krishna, N.R., Agresti, D.G., Glickson, J.D. and Walter, R., Biophys. J., 24 (1978) 791.
40 Boelens, R., Koning, T.M.G. and Kaptein, R., J. Mol. Struct., 173 (1988) 299.
41 Borgias, B.A. and James, T.L., Methods Enzymol., 176 (1989) 169.
42 Gorenstein, D.G., Meadows, R.P., Metz, J.T., Nikonowicz, E.P. and Post, C.P., In Bush, C.A. (Ed.) Advances in Biophysical Chemistry, JAI Press, London, U.K., 1990, pp. 47–124.
43 Mertz, J.E., Güntert, P., Wüthrich, K. and Braun, W., J. Biomol. NMR, 1 (1991) 257.
44 Xu, Y., Sugár, I.P. and Krishna, N.R., J. Biomol. NMR, 5 (1995) 37.
45 Xu, Y., Krishna, N.R. and Sugar, I., J. Magn. Reson., B107 (1995) 201.
46 Bonvin, A.M.J.J., Boelens, R. and Kaptein, R., Biopolymers, 34 (1994) 39.
47 Xu, Y. and Krishna, N.R., J. Magn. Reson., B108 (1995) 192.
48 Yip, P. and Case, D.A., J. Magn. Reson., 83 (1989) 643.
49 Borgias, B.A. and James, T.L., J. Magn. Reson., 79 (1988) 493.

Appendix

Fast exchange

For the particular case of conformational exchange fast on the relaxation rate and chemical-shift scales, a simple expression describing the general behavior of inter-TrNOESY can be derived [14]. In this case Eq. 8 reduces to a *compressed* intensity matrix [11,14] given by

$$\mathbf{I} = \exp\{-\langle\mathbf{R}\rangle\tau\}\,\mathbf{I}_0 \tag{A1}$$

where, for the two-state case,

$$\mathbf{I} = \begin{bmatrix} \mathbf{I}^{L-L} & \mathbf{I}^{L-M} \\ \mathbf{I}^{M-L} & \mathbf{I}^{M-M} \end{bmatrix} \tag{A2}$$

$$\begin{aligned} \langle\mathbf{R}\rangle &= \mathbf{R}_1\mathbf{P}_1 + \mathbf{R}_2\mathbf{P}_2 \\ &= \begin{bmatrix} \mathbf{R}_1^L & 0 \\ 0 & \mathbf{R}_1^M \end{bmatrix}\begin{bmatrix} \mathbf{P}_1^L & 0 \\ 0 & \mathbf{P}_1^M \end{bmatrix} \\ &+ \begin{bmatrix} \mathbf{R}_2^L & \mathbf{R}_2^{LM} \\ \mathbf{R}_2^{ML} & \mathbf{R}_2^M \end{bmatrix}\begin{bmatrix} \mathbf{P}_2^L & 0 \\ 0 & \mathbf{P}_2^M \end{bmatrix} \\ &= \begin{bmatrix} (p_1^L\mathbf{R}_1^L + p_2^L\mathbf{R}_2^L) & p_2^M\mathbf{R}_2^{LM} \\ p_2^L\mathbf{R}_2^{ML} & (p_1^M\mathbf{R}_1^M + p_2^M\mathbf{R}_2^M) \end{bmatrix} \end{aligned} \tag{A3}$$

where $\mathbf{R}_1$ and $\mathbf{R}_2$ are generalized relaxation rate matrices for the free and bound states of the system, respectively, and $\mathbf{P}_1$ and $\mathbf{P}_2$ are the corresponding generalized population matrices [14]. They consist of the submatrices $\mathbf{P}_1^L = p_1^L\,\mathbf{1}_L$, $\mathbf{P}_1^M = p_1^M\,\mathbf{1}_M$, $\mathbf{P}_2^L = p_2^L\,\mathbf{1}_L$, and $\mathbf{P}_2^M = p_2^M\,\mathbf{1}_M$, with fractional populations p_1^L, p_1^M, $p_2^L = 1 - p_1^L$ and $p_2^M = 1 - p_1^M$. $\mathbf{R}_1^L$ and $\mathbf{R}_1^M$ are the relaxation rate matrices for the ligand and the macromolecule in their free state. For the bound state, the corresponding matrices are $\mathbf{R}_2^L$ and $\mathbf{R}_2^M$. The intermolecular cross-relaxation in the complex is represented by $\mathbf{R}_2^{LM}$(and its transpose $\mathbf{R}_2^{ML}$). The intensity matrix $\mathbf{I}$ consists of four submatrices representing intraligand $\mathbf{I}^{L-L}$, ligand–macromolecule $\mathbf{I}^{L-M}$, macromolecule–ligand $\mathbf{I}^{M-L}$, and intramacromolecule $\mathbf{I}^{M-M}$ NOESY matrices. Only one set of resonances for the ligand and one set for the enzyme are visible under the fast exchange condition. From a Taylor series expansion of $\mathbf{I}$, the first few terms of $\mathbf{I}^{L-M}$ are given by

$$\begin{aligned} \mathbf{I}^{L-M} = \mu[M_2]\,\{&-\mathbf{R}_2^{LM}\tau + [(p_1^L\mathbf{R}_1^L + p_2^L\mathbf{R}_2^L)\mathbf{R}_2^{LM} \\ &+ \mathbf{R}_2^{LM}(p_1^M\mathbf{R}_1^M + p_2^M\,\mathbf{R}_2^M)]\tau^2/2! - \mathbf{O}(\tau)\} \end{aligned} \tag{A4}$$

where $[M_2] = p_2^M\,[M_t]$ is the concentration of the bound macromolecule, μ is a constant of proportionality, and $O(\tau)$ represents higher-order terms in τ. A similar expression can be derived for the intra-TrNOESY [11]:

$$\begin{aligned} \mathbf{I}^{L-L} = I^{L-L}(0)\{&1 - (p_1^L\,\mathbf{R}_1^L + p_2^L\,\mathbf{R}_2^L)\tau \\ &+ [(p_1^L\,\mathbf{R}_1^L + p_2^L\,\mathbf{R}_2^L)^2 \\ &+ p_2^M\,\mathbf{R}_2^{LM}\,p_2^L\,\mathbf{R}_2^{ML}]\tau^2/2! - O(\tau)\} \end{aligned} \tag{A5}$$

where $I^{L-L}(0)$ is proportional to the concentration of the ligand.

As noted in the text, the intermolecular intensity I^{L-M} in Eq. A4 is in fact the sum of four separate NOESY contributions: the direct peak $L_2 \leftrightarrow M_2$, the pseudo-direct peak $L_1 \leftrightarrow M_1$, and two exchange-mediated peaks $L_1 \leftrightarrow M_2$ and $L_2 \leftrightarrow M_1$ [4,26]. Of these, the direct peak $L_2 \leftrightarrow M_2$ and the exchange-mediated peak $L_1 \leftrightarrow M_2$ are predicted to be substantially stronger than the remaining two (see Eq. 21B in Ref. 14). Observation of these four individual contributions is possible only if the conformational exchange is slow on the chemical-shift scale. Even though, technically speaking, the $L_2 \leftrightarrow M_2$ contribution (under negligible exchange) is not a transferred effect but a direct effect, we also include this contribution in our definition of inter-TrNOESY. This is reasonable since, under fast exchange conditions, the $L_2 \leftrightarrow M_2$ NOE in the bound state is also influenced. For a three-state model of the type $L_1 + M_1 \rightleftarrows L_2M_2 \rightleftarrows L_3\,M_3$ (e.g., enzymes with hinge-bending motions), it is easily shown that the effective rate matrix $\langle\mathbf{R}\rangle$ is given by $\langle\mathbf{R}\rangle = \mathbf{R}_1\mathbf{P}_1 + \mathbf{R}_2\mathbf{P}_2 + \mathbf{R}_3\mathbf{P}_3$ [14].